Microscopic and macroscopic effects of surface lubricant films in granular shear

Robert G. Cain,[1,*] Neil W. Page,[1] and Simon Biggs[2]
[1]*Department of Mechanical Engineering, University of Newcastle, Newcastle, NSW, 2308 Australia*
[2]*Department of Chemistry, University of Newcastle, Newcastle, NSW, 2308 Australia*
(Received 1 May 2000)

Experiments were conducted to investigate the link between particle-particle interaction forces and the bulk properties of granular shear using an idealized system of near-spherical, monosized glass beads. The atomic force microscopy colloidal probe technique was employed to investigate the adhesion and friction between a single bead and a second glass surface, while the annular shear cell was used to measure the shear properties of the bulk granular material. A covalently bound monomolecular film of aliphatic chains was introduced to alter the tribological interactions between the particles. The atomic force microscope was used to measure the reduction in the particle-particle surface forces resulting from the addition of the boundary lubricant, while the shear cell showed that the effect of the lubricant film was to reduce the coefficient of internal friction and the dilation during shear. This is an experimental study to provide quantitative data linking particle-particle interaction forces and the shear properties of a granular body.

PACS number(s): 83.70.Fn, 61.43.Gt, 81.20.Ev

I. INTRODUCTION

Shear in dry granular materials is a complex phenomenon. Consider, for example, the range of processes occurring at various length scales in a granular body. At the single-particle level, the solid-phase properties of elasticity, plasticity, and toughness are important. At the particle-particle level, if the interfaces slide and roll past one another, the tribological properties of friction, adhesion, and wear are important, while in static contact, chemical reactions at the interface can alter the bulk properties of the assembly. On slightly longer length scales stress chains become important, and the bulk responses of dilation and contraction become evident. Finally, considering the bulk material, some regions may be in motion while others are static, and between these regions complex transitions can occur.

Traditionally, this complexity has meant that granular materials have been modeled as a continuum. The basic assumption used is that, as with fluids and monolithic solids, there exist length scales above which fluctuations at the microscopic level may be ignored. In this way, useful predictions of a granular material's bulk properties can be made with no reference to its discrete nature.

This is not to suggest that the correlations between the properties of the individual particles and the bulk material have been ignored. For example, differences in particle morphology can be related with some confidence to differences in granular behavior [1,2]. Furthermore, computer simulations of granular mechanics are providing significant insights into the links between the properties of individual particles with those of the bulk material [3,4].

However, while the effects of single-particle interaction properties on the bulk mechanical behavior is of significant interest, it is an area of study which has received little experimental attention. Wolfrum and Ponjee [5,6] altered the surface properties of metal and metal oxide powders using a covalently bound lubricant film and found this altered the compaction properties of the bulk powder. However, this study did not include a direct investigation of the particle-particle interaction properties. In another study, Mullier, Tuzun, and Walton [7] developed a single-particle friction cell for measuring contact frictional properties of granular materials, a device which allows internal and wall friction measurements of particles down to 500 μm in size with an accuracy of 0.01 N. Their measurements of normal and tangential compliance during microslip and the internal and wall friction coefficients were found to have a number of implications in the simulations of the flow of granular materials.

The current work describes a significant extension to this idea. The atomic force microscope (AFM) [8] allows adhesion and friction measurements to be made using particles 1–30 μm in diameter. This approach combines two branches of force work being conducted with the AFM: nanotribology (adhesion, friction, lubrication, and wear at the nanoscale [9–15]) and colloidal physics (the interactions of colloidal particles with a second surface—primarily although not exclusively in the normal direction [16–21]).

The approach taken in the current work was to not only quantify the tribological interactions at the particle-particle level using an AFM, but also to manipulate it through the addition of a boundary lubricant. The lubricant employed was identical to that of Wolfrum and Ponjee: a covalently bound monolayer of aliphatic chains. This coating is shown to alter the magnitude of the particle-particle interaction forces. Hence it was a means of manipulating the tribological component of granular shear: the interaction forces as particles slide and roll past one another. The annular shear cell was used to quantify the effects of the lubricant in the bulk material. The work presented here represents an important step in our understanding of the fundamental role of surface films in a sheared granular material.

II. EXPERIMENT

A. Materials

Points of contact within granular systems occur between two surfaces which are geometrically characterized by local

*Corresponding author.
Email address: mergc@alinga.newcastle.edu.au

relative curvature. For a given normal load, this curvature determines the stress field in the contact region. For simplicity in the present work, the standardized geometry of a sphere on a plane was chosen to study the particle level tribology. As will be shown, the normal loads considered in the AFM experiments generated contact stresses of the order of the contact stresses in the shear cell and were sufficient to cause a wide range of tribological features, including lubricant film failure.

To further simplify the study, near-spherical, soda-lime glass beads (Polysciences) were used in both the AFM and annular shear cell. In the AFM experiments, individual beads were selected from a sample with nominal diameters in the range 10–30 μm. These were glued to AFM cantilevers using a two-part epoxy resin. For the shear cell experiments, sieved (150–180 μm) glass beads were used.

The vitreous silica plates used in the AFM experiments were made from Suprasil silica and were supplied polished to optical smoothness (H. A. Groiss, Australia). The AFM was used to determine their surface roughness. Images of the surfaces revealed that in a $2.5\times2.5\,\mu m^2$ scan the standard deviation of the height within the scan area around the mean value was 0.6 ± 0.2 nm. In a $10\times10\,\mu$m scan, the standard deviation was 1.2 ± 0.4 nm. The applied load during imaging was -3 ± 2 nN. These loads were calculated from *force curves* recorded before and after each image. AFM force curves and their interpretation are discussed in Sec. II D.

B. Surface condition preparation and assessment

Unlubricated and lubricated surfaces were prepared for use in both the shear cell and AFM. The unlubricated silica surfaces were prepared via a 20-min sulphochromic treatment [22]. This preparation both cleans the surface and increases the density of surface silanol groups, resulting in an extremely hydrophilic surface on which a sessile water drop produced a thin wetting film. Colloidal probes were cleaned prior to use by exposure to ultraviolet radiation for 1–2 min.

The surface lubricant film was formed via a chemical reaction between the surface hydroxyl groups and stearic (octadecanoic) acid. After the reaction, the surfaces were covered with a monomolecular layer of aliphatic chains. This coating technique is similar to that described by Wolfrum and Ponjee [6] with the exception that the surfaces were first cleaned in sulphochromic acid to fully hydroxylate the surfaces. A magnetic stirrer was employed when cleaning the beads to prevent agglomeration. After cleaning, the materials were washed several times in water and dried in vacuum.

To coat the surfaces, the material was suspended in a solution of 1 wt % stearic acid in mesitylene (1,3,5-trimethyl benzene). The beads were again stirred to prevent agglomeration. Nitrogen was passed through the system for up to an hour to form an inert atmosphere, before heating the solution to 100 °C at which it was maintained for at least 3 h.

Following the coating procedure, the surfaces were washed several times with hot (50–60 °C) toluene to remove the unreacted physisorbed acids. The sample was then dried and stored in vacuum. Contact angle measurements showed no variation with time when the surfaces were stored this way. The diffuse reflectance infrared Fourier transform (DRIFT) spectra method was used to determine whether the expected reaction had taken place. It showed a metal stearate stretching frequency at 1570 cm^{-1} and C-H bonds around 2900 cm^{-1}. No unreacted carboxylic acid which would cause a peak at 2900 cm^{-1} was indicated.

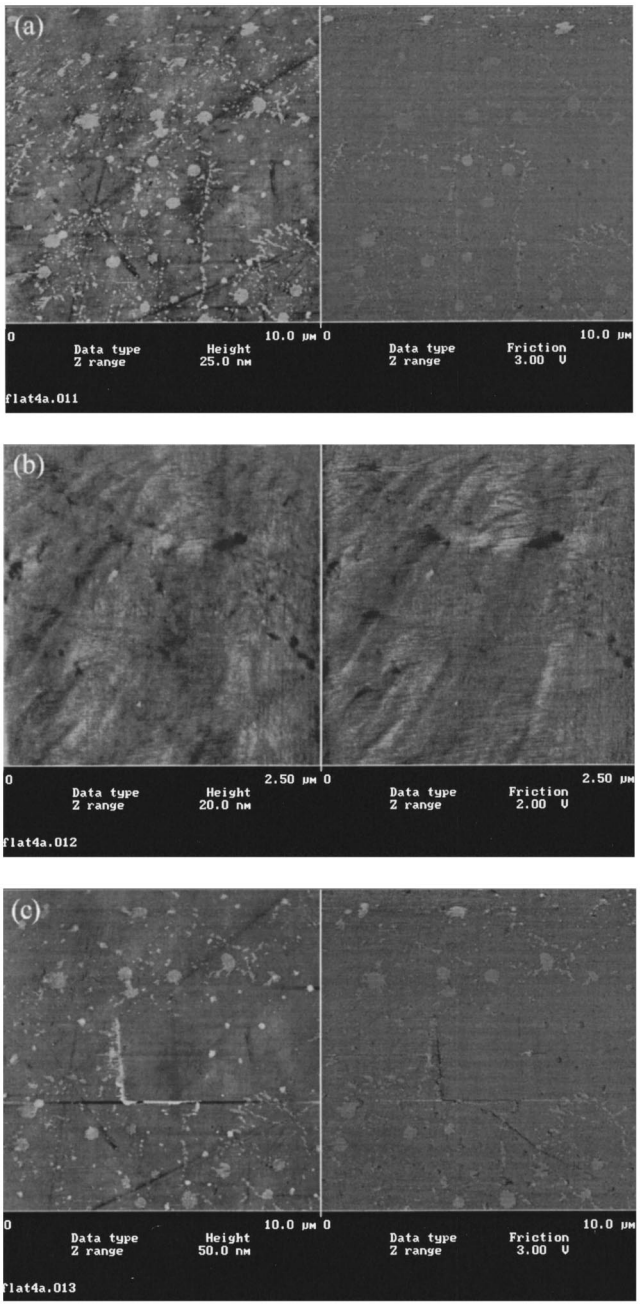

FIG. 1. Three AFM images of a coated silica flat which show the lubricant coverage and the ease with which the surface films can be damaged under an AFM tip. (a) 10-μm scan at an applied load of 1 ± 2 nN. (b) 2.5-μm scan at an applied load of 36 ± 2 nN. (c) 10-μm scan at an applied load of 1 ± 2 nN over the same region as (a). The square where image (b) was recorded is visible in the center.

The AFM was also used to characterize the lubricant film, first to determine the film coverage and, second, to qualitatively explore the film's resistance to wear. A series of three images is shown in Fig. 1. Each consists of two data sets: the height (or AFM) data on the left and the friction

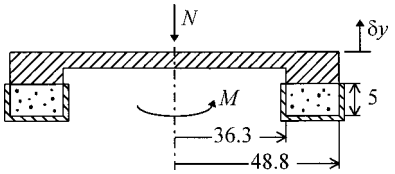

FIG. 2. Schematic of the annular shear cell used in the bulk shear property studies. A normal load N is applied to the lid and the torque M necessary to restrict the lid from rotating is recorded. Changes in the height of the lid, δy, are also monitored. Dimensions are in millimeters. Since the particles were sieved to 0.15–0.18 mm, the width and depth of the test sample were approximately 75 and 30 particle diameters, respectively. This is sufficient to remove ''edge'' effects due to the confining surfaces [23].

(or LFM) data on the right. Variations in height and friction are indicated by variations in gray scale: in the AFM image, the higher the topographical element, the lighter the tone, and in the LFM image, the lighter the tone, the greater the interface shear resistance.

Figure 1(a) is a $10\times10\ \mu m^2$ image, scanned at an applied load of 1 ± 2 nN. The origins of the lighter patches, resembling splashes on the surface of the plates, are unknown. From the AFM and LFM images, these regions appear to be higher and have a higher friction.

Figure 1(b) is a $2.5\times2.5\ \mu m^2$ image, scanned at a significantly higher applied load of 36 ± 2 nN. Note that the detail present in the previous image is lost. Finally, Fig. 1(c) is a $10\times10\ \mu m^2$ image, once again scanned at 1 ± 2 nN. It is of the same region as Fig. 1(a). Some of the same distinguishing features can be seen in both images (a) and (c). However, in image (c), the $2.5\times2.5\ \mu m^2$ square from the imaging of image (b) is clearly visible in the center. Hence, at the higher applied load, the surface film is damaged by the tip. Indeed, the lubricant has been mechanically removed and lies in a small pile at the edge of the imaged square.

These images indicate the lubricant film does not provide a perfect coverage. In the $10\times10\ \mu m^2$ image area, there are many regions of higher friction. It is interesting to note that imaging at the lower applied load did not appear to degrade either these marks or the lubricant film. However, at the higher applied load, the surface stearate film has been mechanically removed. This behavior will be discussed in more detail in Sec. III, in which the frictional characteristics of the lubricant film are examined in a more quantitative fashion.

C. Shear cell

A Wykham Farrance ring shear cell was used to conduct the annular shear cell experiments. As illustrated in Fig. 2, a load was applied to the upper platen, and as the annulus rotated, the torque necessary to prevent the upper platen from rotating was recorded. To ensure that failure occurred within the granular material and not at the sample/platen interface, emery paper with a mean grit size similar to the dimensions of the glass beads was glued to the surface of the upper platen. The success of this procedure could be assessed in two ways. First, the shear response of granular-wall friction is significantly different to granular internal friction; granular wall friction is associated with flat and abrupt peak shear strengths [23]. Second, by carefully pouring the granular material from the lower platen following a shear cell test, the loose material in and above the shear zone would flow easily out before the compacted material below. If there were a reasonable amount of this material, it was safe to assume that failure did not occur at the platen/sample interface.

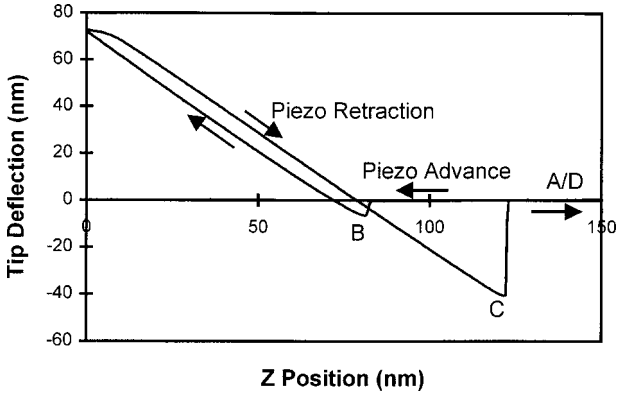

FIG. 3. AFM force curve recorded between a clean hydrophilic silica glass colloidal probe and a similarly treated silica surface, with arrows indicating the advancing and retracting piezo traces. Figure lettering is explained in the text.

The changes in height of the sample were also recorded. This device was designed by Bromhead primarily for geotechnical analysis [24] in which the emphasis is on the measurement of the sustained yield locus. However, it has been shown that with careful design of the experimental technique, the annular shear cell can give measurements of the peak shear strength in excellent agreement with those of linear testers [25,26]. In the present work, the experimental procedure of Wilms and Schwedes is followed [25].

D. Atomic force microscopy

A Nanoscope III (Digital Instruments) Multimode AFM was used to conduct the particle friction and adhesion experiments. The calibration of the AFM has been described elsewhere [27]. Individual beads, in the 10–30 μm size range, were attached with a two-part epoxy resin to the end of single-beam, etched silicon cantilevers (Digital Instruments, model TESP).

The cantilever probe was mounted in a Digital Instruments fluid cell in a clean laminar flow cupboard and the assembly was then installed in the AFM. High-purity nitrogen (BOC gas code No. 034) was passed through the fluid cell containing the sample and cantilever probe for approximately 30 min prior to an experiment. A slight positive pressure was maintained throughout the experiment to ensure no ingress of atmospheric air.

Two basic modes of operation were employed in the quantitative AFM force work; the first gives a *force curve* and the second a *friction loop*. An example of a force curve for a clean, hydrophilic glass bead interacting with a similarly treated silica glass flat, is shown in Fig. 3. Force curves plot cantilever deflection versus sample position as the piezo advances and retracts the silica flat, making and breaking contact with the bead attached to the cantilever. The arrows in Fig. 3 indicate the direction of travel. The Z position zero is defined by the maximum height to which the sample is driven by the piezo. At A, the two surfaces are a significant distance from each other and there is no interaction between

the two. As the sample nears the surface, the van der Waals attraction results in the two surfaces jumping into contact at *B*. The sample and bead, then in contact, move together in the compliance region. On retraction, the surfaces stay in contact until the adhesive force is matched by the spring force at *C*, and the surfaces separate. At *D* the surfaces are again a significant distance from one another and there is no interaction between the two. For the purposes of this study, a ''good'' force curve has a flat and sufficient base line to define zero tip deflection, since this corresponds to zero interaction between the surfaces. It also has a compliance region sufficient to calibrate the photodiode response to tip deflection and, hence, determine the applied and measured forces between the interacting surfaces. Finally, the force curve should be conducted on a scale of similar order to the adhesive forces between the surfaces.

The result shown in Fig. 3 is typical of the interactions between clean, dry, hard surfaces [28,29]. In the following section, results are presented which demonstrate the important role the lubricant film plays in altering these interactions.

The second mode of operation, in which the silica flat is rastered from side to side under the bead, gives the friction data. The interpretation of the resulting friction data is described elsewhere [27]. Force curves were captured before and after each set of friction experiments. These were necessary in order to calibrate the applied load during the friction experiments. However, they also provide important information regarding the nature of the surface interactions. A ''set'' of friction experiments involved a series of friction loops being recorded over a range of applied loads. Each friction loop gives the friction force for a particular applied normal load. Typically, the first of these friction loops was recorded at or near zero applied load. The photodiode voltage corresponding to zero cantilever displacement, and hence zero applied load, was established from the force curves prior to commencing the friction experiments. The load was then increased in small increments and friction loops were recorded at each setting. The maximum load which could be applied was a function of the normal stiffness of the cantilevers ($20\pm2\ \mathrm{N\,m^{-1}}$) and the maximum normal cantilever deflection prior to the signal going off scale, limited by the alignment of the detector system. The effect of varying the maximum applied load on the frictional response was not investigated. The load was then decreased until the surfaces separated, frequently under a negative applied load. This is a result of the complex interaction between friction and adhesion. The results to be presented here show that altering the surface chemistry alters both the frictional response and the adhesive forces between the surfaces. Furthermore, friction testing was found to damage the surface films, further complicating the interactions between the surfaces.

III. ATOMIC FORCE MICROSCOPY RESULTS

The purpose of the AFM friction experiments was to compare the interaction properties of the unlubricated and lubricated surfaces. This was achieved by gluing a bead with the surface chemistry of interest to an AFM cantilever and measuring its adhesion and frictional properties against a surface with the same surface pretreatment. Two sets of measurements are presented: first between clean, hydrophilic silica surfaces and, second, between silica surfaces coated in a covalently bound, monomolecular lubricating layer of aliphatic chains.

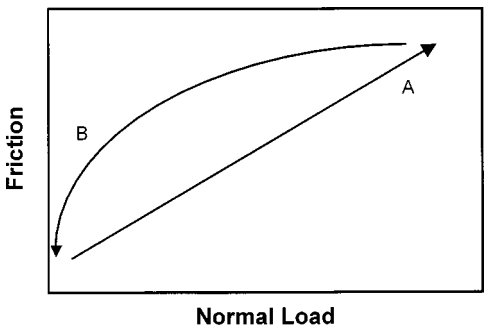

FIG. 4. Frictional behavior of unlubricated surfaces. Path *A* is the initial near-linear dependence of friction on applied load as the load was increased from zero to its maximum value. Path *B* is the frictional response as the load was decreased or for any subsequent testing over the same wear track.

A. Unlubricated surfaces

The characteristic frictional response of the unlubricated surfaces is summarized in Fig. 4. There was an initial linear dependence of friction on applied load as the load was increased. This is path *A* in Fig. 4. These results are shown in Fig. 5 for five different probes with radii 10–12.5 μm. A least-squares fit of these results to a linear relation of the form $F=\mu P+F_0$, where F is the friction force and P the normal load, gives a coefficient of friction of $\mu=1.83\pm0.13$ and friction at zero applied load, $F_0=510\pm150$ nN. This value for the coefficient of friction appears high. ''Macroscopic'' measurements of the coefficient of friction of glass on glass from the literature show that its value depends on the cleanliness of the surfaces. When glass surfaces are freshly formed or, as with the present work, they are chemically cleaned, the coefficient of friction may reach unity [30]. However, the measurements reported here differ significantly from previously reported experiments because of the rela-

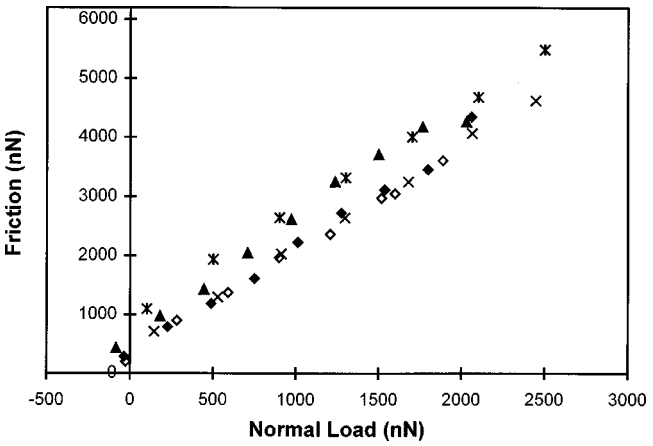

FIG. 5. Initial frictional response of the unlubricated surfaces for five different colloidal probes with bead radii 10–12.5 μm. These results correspond to path *A* in Fig. 4.

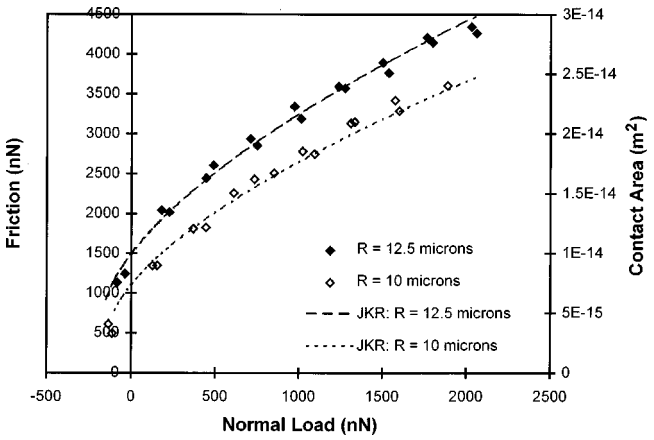

FIG. 6. Response of two unlubricated probes subsequent to the wear track being fully developed. This corresponds to path *B* in Fig. 4. The contact area, calculated using JKR theory, is also shown.

tively small size of the beads and the high contact stresses involved. Due to the acute radii of curvature, the surface topographical features may be comparable in size to the gross body dimensions. Hence it is reasonable that their frictional characteristics differ significantly from those displayed by gross bodies [31]. Kendall has reported that for such extreme cases the friction coefficient can be double that reported at high loads in macroscopic experiments, due to the interaction between surface adhesion and friction [32]. This phenomenon will be discussed in more detail shortly.

Decreasing the normal load or, indeed, for any subsequent testing over the same wear path, the friction force showed a significantly different response. This is path *B* in Fig. 4. For clarity, only two examples of this behavior are shown in Fig. 6. For reasons which will be discussed below, the contact area during sliding is also plotted for these two beads, calculated using the Johnson-Kendall-Roberts (JKR) theory of contact mechanics [33],

$$a^3=\frac{R}{K}[P+6\gamma\pi R+\sqrt{12\gamma\pi RP+(6\gamma\pi R)^2}], \qquad (1)$$

where a is the contact radius, from which the contact area may be determined, R is the radius of the sphere, K is the bulk elastic modulus, P is the applied load, and γ is the surface energy.

The simple linear relationship between the frictional response of two surfaces and their true area of contact is well established [34–36]. Furthermore, for a wide range of surfaces, the JKR theory of contact mechanics has been found to accurately predict the area of contact between smooth spheres and flat surfaces while accounting for the adhesion between those surfaces [35]. The results presented in Fig. 6 indicate that for these worn hydrophilic surfaces, the frictional response is that of a smooth sphere sliding on a smooth flat surface. The fit in Fig. 6 was achieved by assuming a linear relationship between the frictional response and the contact area predicted by Eq. (1). It used the true radii of the two spheres, $R=10$ and 12.5 μm, and the bulk elastic modulus $K=49$ GPa, calculated from the material properties of the soda lime glass beads and the silica flats [30]. The fitting parameter was the surface energy, which gave $\gamma=0.0015\ \mathrm{J\,m^{-2}}$. This value is less than the surface energy calculated from pull-off curves, which varied from 0.0025 to 0.0075 $\mathrm{J\,m^{-2}}$. It is also less than those measured by Vigil *et al.* for atomically smooth silica surfaces in sliding contact of 0.005–0.015 $\mathrm{J\,m^{-2}}$ [37]. These variations are most likely due to the initial roughness of the two contacting surfaces, which is known to have a significant influence on measurements of surface energy [35].

It is well established that friction is proportional to the true area of contact. Furthermore, relations between the roughness of two contacting surfaces and the frictional dependence of those surfaces in sliding contact are well developed. For example, from Archard's analysis of an arbitrary contact [38], the friction force F may be written

$$F\approx kP^n, \qquad (2)$$

where k is a constant dependent on the form and elastic properties of the surfaces, P is the applied load, and the index n also depends on the surface roughness. For Hertzian contacts, $n=2/3$, but as the number of asperity contacts within a given contact region increases, n approaches unity, from which Amonton's law follows.

An explanation for the form of the results in Figs. 5 and 6 follows from this. Initially and as the load is incrementally increased to its maximum value, the surfaces contact at a number of asperity contacts. While it is impossible to determine how many contacts form between the surfaces, the significant cohesion, or friction at zero applied load, suggests it may be very few. This would also explain the relatively high coefficient of friction displayed during the initial loading. Although the surfaces are not ''smooth,'' adhesion clearly plays a crucial role in the frictional interaction. Hence fitting a straight line to the data may be misleading. Rather, it may be that insufficiently high loads have been applied to reveal any curvature in the frictional response.

However, subsequent to the maximum load being applied, the frictional response follows a different, clearly nonlinear path. This result indicates that the contact region changes during friction testing: with repetitive testing, the number of contact points is reduced. That is, the contact undergoes a transition from multiple asperity to single-region contact during the loading cycle. This unusual result is consistent with the following mechanism. On the surface of hydrophillic silica is a relatively soft, gel-like layer of intertwined polymeric chains of $Si(OH)_2$-O-$Si(OH)_2$-OH. Previous studies have shown this film to be around 1–2 nm thick [37], roughly the same dimension as the surface irregularities on the polished flats. Under the high pressures applied here, asperities in the silica gel layer are smeared out, reducing the number of contacts between the surfaces. Note that this response was found to occur only if all the testing were concentrated on one wear track and only subsequent to the maximum applied load being applied. The frictional response then indicated that contact between the surfaces on the worn track was made over a single region, as opposed to the multiple asperity contact of the initially rough surfaces.

The limitation of Archard's analysis is that it ignores the effects of adhesion between the surfaces. The JKR theory describes the more sophisticated relationship between ap-

plied load and contact area when adhesion is also present. This theory was used to estimate the contact area consistent with the friction response in Fig. 6. The experimental results match the predicted form of the area of contact extremely well. This suggests that, as a first approximation, the worn contact region may indeed be described as the interface of two ''smooth'' surfaces.

Of course, the JKR theory is not the only theory developed to describe the elastic contact of smooth surfaces. The applicability of the JKR model depends on the value of a nondimensional parameter [35]

$$\mu_t = \left(\frac{R w_0^2}{E^{*2} z_0^3} \right)^{1/3}, \tag{3}$$

where R is the radius of the sphere, w_0 is the work of adhesion (= twice the surface energy γ), z_0 is the equilibrium spacing in the Lennard-Jones potential and $E^* = [(1-\mu_1^2)/E_1 + (1-\mu_2^2)/E_2]^{-1}$ is the combined elastic modulus, where E_i and μ_i are the Young's modulus and Poisson's ratio of surface i respectively. The parameter μ_t is a measure of the magnitude of the elastic deformation compared with the range of surface forces. Johnson found that for sliding contacts, the JKR theory predicted the contact area acceptably well for values of μ_t greater than about 0.2 [35]. In the present work, $R = 10\,\mu$m, $z_0 \approx 0.2$ nm [35], $E^* = 38$ GPa, and from the pulloff forces, $w_0 = 0.01 \pm 0.005\,\mathrm{J\,m^{-2}}$, and hence μ_t is 0.3–0.6. Therefore, if the surfaces are contacting at a single region of contact, the JKR theory should describe the contact geometry.

The JKR contact area modeling also allows the peak contact pressures generated during friction testing to be calculated. From Hertzian analysis, the peak stress σ_0 encountered between a sphere and a flat being pressed together by load P is given by [39]

$$\sigma_0 = \frac{3P}{2A}, \tag{4}$$

where A is the true area of contact. In the friction experiments illustrated in Fig. 6, the 10 μm radius sphere suffers a maximum applied load P of approximately 2000 nN, at which the contact area was around $2.5 \times 10^{-14}\,\mathrm{m^2}$. Hence the peak stress is this case was approximately 120 MPa, which is sufficient to plastically deform the relatively soft gel-layer on the glass surfaces [37].

These results highlight the complex role of surface films in the frictional interactions of particulate media, even in dry conditions. In the next section, the frictional interactions are considered for surfaces with two surface films: the ''natural'' silica gel layer and the introduced monolayer of aliphatic chains.

B. Lubricated surfaces

Results with the lubricated silica surfaces also indicate that the interactions and degradation of the surface films strongly influence the frictional response. Figure 1 showed that the lubricant film could be damaged by the interaction with the AFM tip, once the applied load exceeded a critical level. Here we examine this effect in more detail.

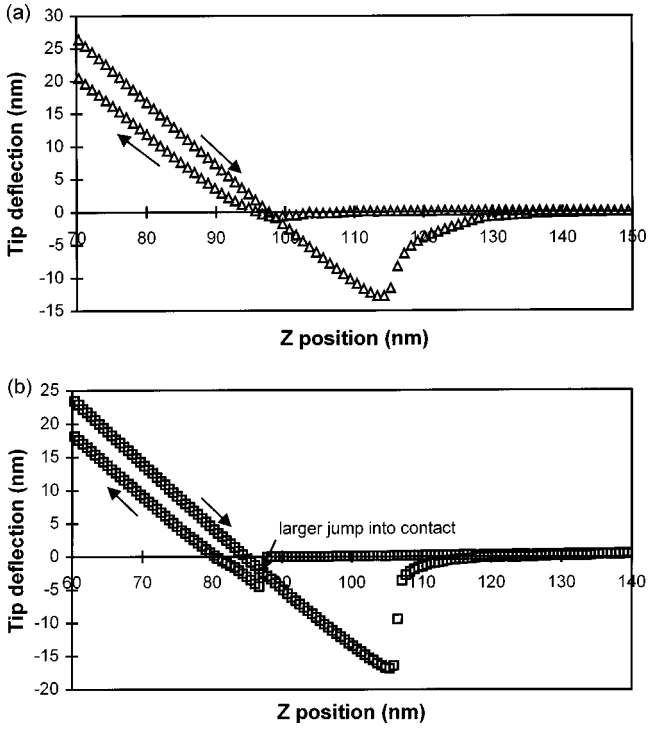

FIG. 7. Force curves recorded (a) before and (b) after the first set of friction experiments. The larger jump into contact on approach and the more abrupt disentanglement on separation suggest damage to the lubricant films in (b).

Two normal force curves are shown in Fig. 7. The first of these was recorded prior to any friction testing between the coated surfaces, and there is evidence of a lubricant coating influencing the surface interactions on advance and retraction. First, the lubricant films reduce the van der Waals attraction between the two surfaces. This can be seen in Fig. 7(a); there is no ''jump'' into contact as the sample approaches the sphere. Second, once contact is made and the surfaces are forced together, the lubricant films intertwine. On retraction, the resulting interdigitation of the surface films must be overcome. This results in a gradual disengagement, which occurs over approximately 20 nm of piezo travel. This is significantly longer than the combined lengths of the two films (2×2.4 nm) [40]. However, the disengagement conditions are complex: the surfaces are not smooth, and as we have seen, the lubricant films are themselves attached to soft films of intertwined polymeric chains which may effect the results. It is also likely that the surfaces peel out of contact rather than pulling cleanly apart. It is therefore not unreasonable that disentanglement takes considerably longer than the combined length of the two films.

The second normal force curve, Fig. 7(b), was recorded after a set of friction tests and shows the effects of some damage to the lubricant film: as the surfaces approach, there is a small jump into contact, and as the sample recedes, the jump out of contact is more abrupt. However, engagement and disengagement do not yet resemble the results with the unlubricated surfaces (Fig. 3). As the friction results below show, it was only through repetitive shearing at these loads that the lubricant films were completely removed.

Figure 8 shows the results of friction testing between the two surfaces. The first two sets of friction data are shown.

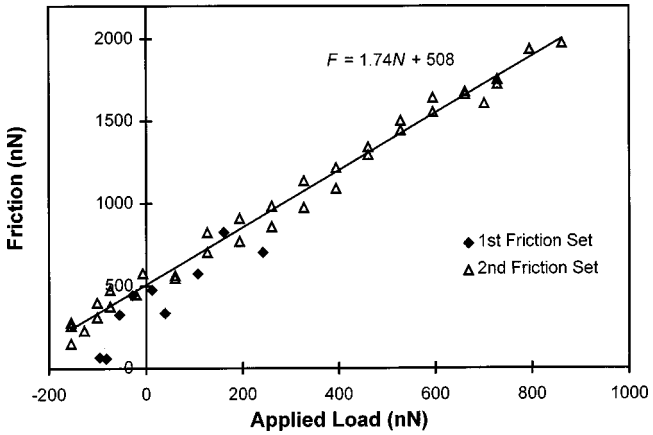

FIG. 8. Friction versus applied load for the first two sets of friction tests on lubricated surfaces.

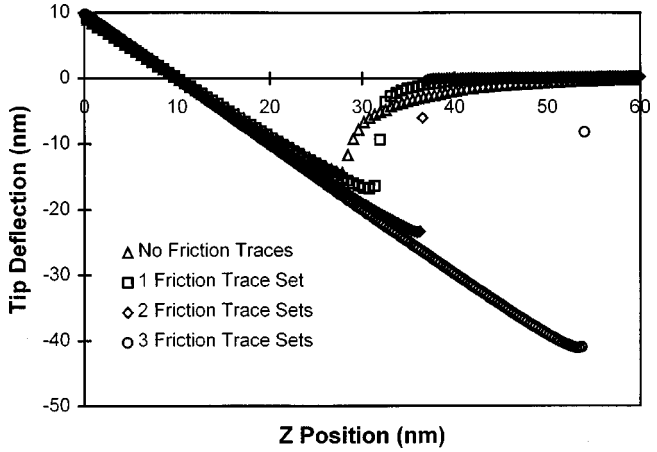

FIG. 9. Tip deflections as the sample retracted, recorded before and after the three sets of friction experiments.

The force curve in Fig. 7(a) was recorded before the ''1st Friction Set''—the solid diamonds in Fig. 8—and the force curve shown in Fig. 7(b) was recorded between this and the ''2nd Friction Set''—the open triangles in Fig. 8.

There is more scatter associated with the first set of results than with subsequent friction experiments. This result is a consequence of the unusual contact mechanics encountered at the interface during the initial testing. In this series of experiments, the surfaces were covered in two soft films: the silica gel layer and the lubricant film. The results in Fig. 7 indicate that the pressures applied during friction testing were sufficient to damage these surfaces (see Sec. III A). As this occurs, the magnitude of the frictional response varies significantly from trace to trace. It is therefore difficult to conclude the magnitude of the lubricating effect of the lubricant film. However, it appears the lubricant film reduces the friction at zero applied load. This is consistent with the reduced adhesion seen in the normal force curve plots.

An interesting result in Fig. 8 is that there is little difference between the frictional response of the ''worn'' lubricated surfaces (for ''set 2,'' $\mu = 1.74$ and $F_0 = 508\,\mathrm{N}$) and the unlubricated surfaces prior to the wear path being fully developed ($\mu = 1.83 \pm 0.13$ and $F_0 = 510 \pm 150\,\mathrm{N}$). This is despite the significant influence the lubricant film still has on the magnitude of the adhesion between the surfaces. This is considered in more detail in Fig. 9, which shows the *retraction half* of the force curves recorded before and after each set of friction traces. The first two, recorded before and after the first sets of friction experiments, have been shown already (Fig. 7). In Fig. 9, the force curves recorded after the second and third sets of friction experiments are also shown. The same trends noted earlier continue in these traces: the pull-off force increases, and the interdigitation of the lubricant films as the surfaces separate decreases. Indeed, the last trace is very similar to the force curves recorded between unlubricated surfaces (Fig. 3). It follows that the final set of friction results should resemble the frictional behavior of two unlubricated, hydrophillic surfaces. As shown in Fig. 10, this is indeed the case. The third set of friction results shows a linear increase in the friction with applied load; then, as the load is reduced, the response resembles the JKR-type behavior seen previously in Fig. 6.

This study demonstrates the significant role of surface films in determining the forces of interaction between a single particle and another surface. This is not a surprising result, although some of the interactions are unusual. In the unlubricated material, we suggest that the surface gel-like layer is particularly important in determining the nature of the frictional response. Repetitive sliding produces a wear path in the soft gel layer. This results in a change in the contact mechanics: the friction at zero applied load increases dramatically, and the frictional response resembles that for a smooth elastic contact and has been modeled using the JKR theory of contact mechanics.

The response of the lubricated surfaces is even more complex. In this case, two surfaces films are present: the soft gel layer and the covalently bound aliphatic chains. The effect of the lubricant film is to reduce the adhesion between the surfaces. However, the film is damaged relatively quickly at the pressures considered here. Hence, although it seems the frictional response is altered by the lubricant film, due to the damage the repetitive testing incurs, it is difficult to establish the virgin film performance. We will return to consider these points in the following section when interpreting the shear cell results.

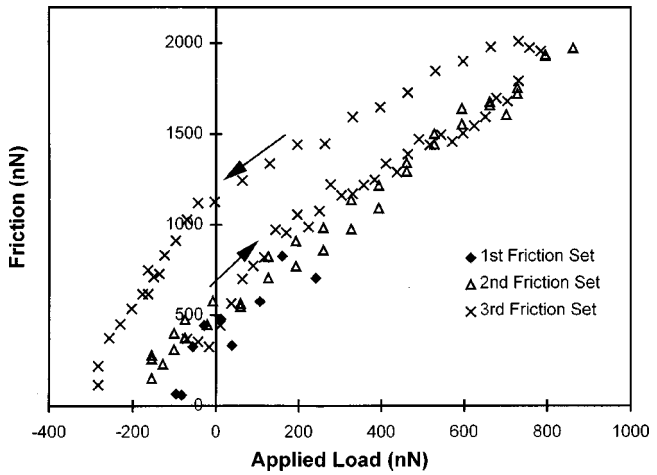

FIG. 10. Friction versus applied load for three sets of LFM tests. The arrows indicate the progressive application of applied load in the third set of friction tests. By this stage, the lubricant appears to have been completely removed and the frictional response is identical to that of the unlubricated surfaces shown in Fig. 5.

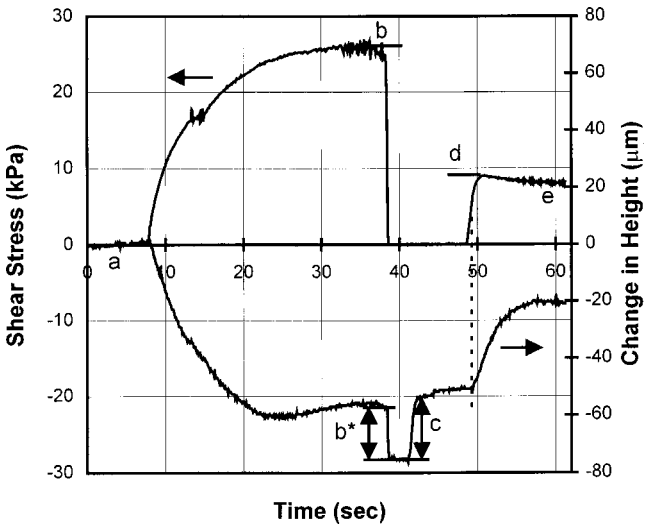

FIG. 11. Shear stress and sample height changes versus time for an annular shear cell experiment. The consolidation pressure was 62.3 kPa and the test normal pressure was 18.1 kPa. Figure lettering is explained in the text.

IV. SHEAR CELL RESULTS

The annular shear cell was used to assess the changes in the shear behavior of a granular material altered exclusively through the manipulation of the surface films on the individual particles: that is, to determine the effect of the known reduction in particle interaction forces on the shear response of the bulk granular material.

In a typical shear cell test, normal loads are applied and the shear strength of the material for given consolidation conditions is recorded. As an example, Fig. 11 is an annular shear cell test on an unlubricated sample, with a 62.3-kPa consolidation pressure and an 18.1-kPa test pressure. Both the shear stress and height of the sample are shown. Referring to the lettering in Fig. 11, shear commences under the consolidation pressure at *a*, and the shear stress and bulk density increase to the steady-state condition corresponding to that applied pressure. At *b*, there is a small amount of stick-slip motion beginning to occur. This phenomenon is considered elsewhere [41,42]. Only the *steady* response of the material will be discussed here.

Once the steady-state condition has been achieved, the shear drive is stopped. Note that the height of the sample does not change; it is not until the shear stress is removed that the shear zone collapses. This is the change in height b^*. This event is known as contraction. While dilatancy and contraction are well-known properties of granular materials, the role interparticle friction plays in the development and collapse of shear zones is poorly understood. To this point, the material is being preconditioned prior to evaluation at the selected test pressure.

At *c*, the applied pressure is reduced to the testing pressure, and the material expands. Following Wilms and Schwedes [25], only that load is removed which reduces the consolidation load to the test load. This promotes the preferred stress distribution in which the maximum shear stress is encountered at every point across the radius simultaneously. At the normal stresses examined here, the relaxation of the sample as the load is reduced is quite significant. Since there is typically little particle rearrangement as the load is reduced [23], a significant portion of this change in height is due to elastic recovery in the granular assembly.

The shear stress is then reapplied. There is a delay before the material begins to dilate, and the shear stress increases almost linearly over this region. This suggests that the material is responding elastically to the applied shear in this region. As dilation in the shear zone starts, the material weakens, although the shear stress continues to increase until a maximum is reached at *d*. This is the *test* shear strength. As the material in the shear zone continues to expand, the shear stress drops to the level associated with the test normal stress, *e*. Shear is then sustained with no further dilation.

Most studies of the shear properties of granular materials are concerned primarily with the strength of the material as normal and shear loads are applied. However, in many applications there is also interest in the material response during the reduction of these loads. At *b* in Fig. 11, the shear stress is removed and the shear zone contracts, while at *c* the applied normal pressure is reduced, and the sample expands. Comparisons and analyses are presented here of these sample responses for the lubricated and unlubricated materials. However, before these are presented, we consider the stress states at the points of contact in the annular shear cell experiments, allowing meaningful comparisons with the tribological properties examined in the AFM experiments.

A. Local stress states

In a shear cell experiment, the true stresses present at the points of contact between particles substantially exceed the apparent or continuum stresses used to characterize the stress state of the bulk granular material. However, it is possible to deduce an approximate relationship between the two. In a real granular material, the true stresses encountered at the points of contact depend on coordination number, size distribution, and particle shape. However, making the assumption of mono-sized spheres in a simple cubic array and ignoring shear stresses at the points of contact, Page showed that the peak contact stress σ_0 is related to the bulk compressive stress σ_{xx} by the relation [43]

$$\sigma_0 = 0.978 E^{2/3} {\sigma_{xx}}^{1/3}, \tag{5}$$

assuming Poisson's ratio $\nu = 0.3$. The soda-lime glass beads used here have a Young's modulus $E = 72$ GPa [30]. For this example, using the test normal pressure in Fig. 11 ($=18.1$ kPa) as the bulk compressive stress, the peak contact stress $\sigma_0 \cong 440$ MPa. This is larger, but of the same order, as the peak stresses applied with the AFM. Conclusions may therefore be drawn regarding the origin of the response of the bulk material in the annular shear cell using the knowledge gained from the AFM experiments of the tribological properties of the lubricated and unlubricated materials.

B. Sample shear strength

The shear strength of the lubricated and unlubricated samples for consolidation loads of 62 and 298 kPa are summarized in Fig. 12. Clearly, there is a significant reduction in the internal friction angle associated with the addition of the boundary lubricant to the material system.

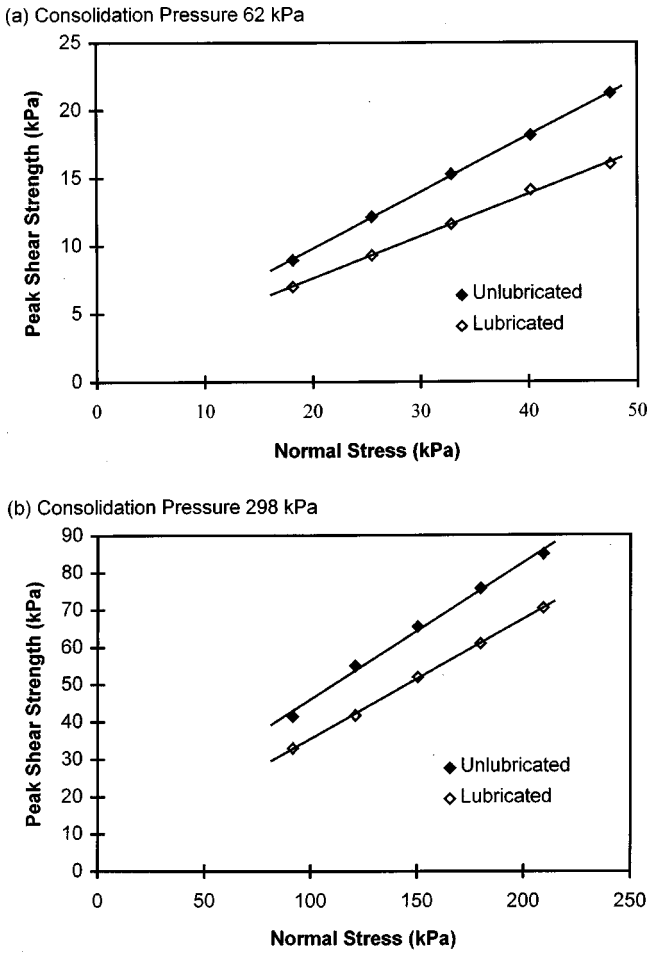

FIG. 12. Comparison of peak shear strengths for lubricated (open diamonds) and unlubricated (solid diamonds) samples at consolidation pressures of (a) 62 kPa and (b) 298 kPa.

From the AFM results, it is known that the lubricant film reduced the surface interaction forces. However, repetitive friction testing also damaged the lubricant film, reducing its effectiveness. By comparison, over the length scales of the shear cell experiments, typically 2–3 mm or approximately 1% strain, there was no appreciable change in the granular shear strength for the lubricated samples. That is, the film was maintaining its effectiveness. This result highlights one of the complexities of this study. In the AFM tests, the contact region between the particle and surface is controlled, and it is possible, within certain limitations, to assess the rate and effect of the destruction of the lubricant film. However, within the shear zone of the granular body, particle-particle contacts occur in a random fashion. Hence, after 3 mm of travel, ''virgin'' contacts are still occurring.

Nevertheless, this is a significant result. It demonstrates that the magnitude of particle-particle interaction forces have a critical role in determining the stress states achieved in the shear of granular materials. While there is a vast body of literature which deals with the importance of particle shape, size, and size distribution [44–48], there are very few experimental data which specifically examine the relative importance of particle-particle interaction forces. For this reason, numerical simulations of granular flow have required a certain amount of guess work in the definition of microscopic interaction properties. In ''rigid particle modeling,'' which is

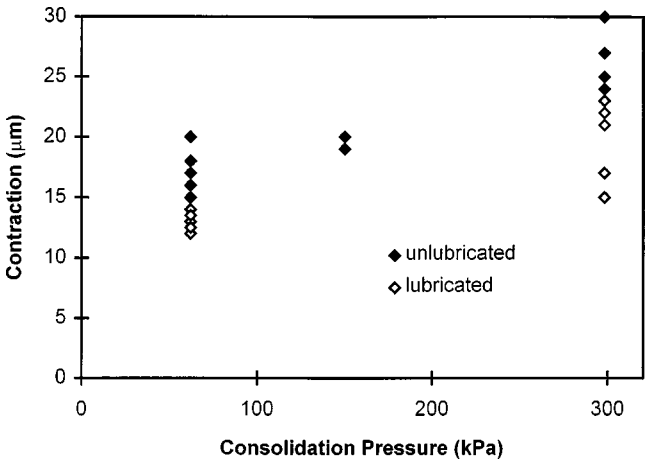

FIG. 13. Contraction, or the drop in height of the sample due to the removal of the shear stress, versus the normal pressure, for lubricated and unlubricated samples.

based on instantaneous particle collisions, the friction coefficient is not defined [3]. Rather, energy is dissipated at the particle-particle level through a coefficient of restitution. It should be noted, however, that this approach is most suited to modeling high-velocity, high-porosity flows. One alternative is discrete element analysis, or ''soft particle modeling'' [31], in which realistic interaction laws between the particles can be incorporated. Simulations of steady shearing using this technique have shown that the stresses depend strongly on the degree of elasticity and porosity, but less on the interparticle friction. However, the present work demonstrates that manipulations of a granular material's particle interaction properties do have a significant effect on the bulk shear properties.

C. Sample response to shear stress removal

When the shear stress is removed, the shear zone collapses or contracts. The measured contraction is the drop in height of the entire sample due to the removal of the shear stress. This is event b^* in Fig. 11. Figure 13 compares the contraction experienced by the lubricated and unlubricated samples at a range of applied loads.

There is considerable scatter in these results, due mainly to a ripple of ± 2 μm in the linear variable differential transducer (LVDT) output, which was used to measure sample height fluctuations. Despite this, these results suggest that (a) the contractions increase with increased applied normal pressure and (b) decrease with the addition of a lubricant film.

The first of these results is a well-known property of granular materials [44] and will not be discussed further here. The more interesting finding is the second, which indicates that particle interaction forces also influence the structure of the shear zone. If it is assumed that due to the identical particle geometry in the two cases the total number of particles involved in the shear process is the same, then the effect of the lubricant must be to decrease the shear zone porosity. This result would occur as a consequence of particles sliding more easily past one another, allowing a more dense packing structure. The alternative is that fewer particles are required in the shear zone of the lubricated material in order to allow shear. That is, the reduced particle interac-

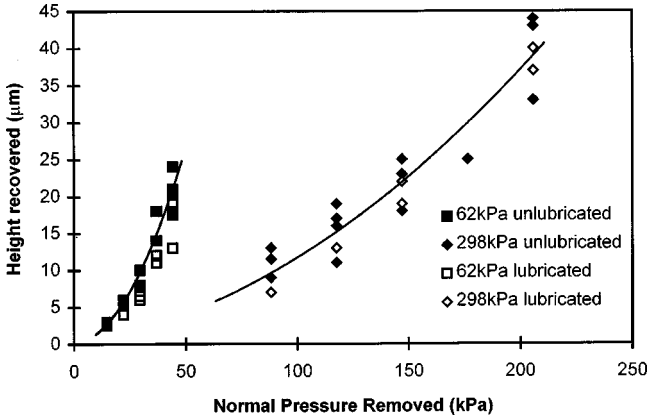

FIG. 14. Height change in the sample versus the normal pressure removed for two different consolidation stresses: 62 and 298 kPa. For example, for a consolidation pressure of 150 kPa, removing 80 kPa means the test normal pressure was 70 kPa. From the figure, as this pressure was removed, a typical sample expanded by around 16 μm. The lines shown are indicative trend lines only.

tion forces allow the formation of a more efficient shear zone structure. However, separating these effects is not trivial. Further work is required to completely describe the effect of surface lubricant films in granular packing, dilation, and shear.

D. Sample response to normal stress reduction

When the applied normal load is reduced, the material expands. This is event *c* in Fig. 11. At the stresses examined here, the relaxations of the sample as the normal load is reduced are quite significant. Figure 14 is a plot of the variation of the height recovered in the sample against the normal pressure removed for two sample consolidation pressures. There is little difference between the lubricated and unlubricated sample relaxations, suggesting the degree of unloading is primarily a function of the load removed and initial density of the sample, rather than being dependent on the tribological properties of the particles.

A simple qualitative comparison with particulate assembly elasticity theory can be used to interpret the trends displayed in Fig. 14. From Kendall [49], the elastic modulus of packings of irregular spheres, E_p, follows the relationship

$$E_p = 17.1\varphi^4\left(\frac{E^2\gamma}{D}\right)^{1/3}. \tag{6}$$

where φ is the packing fraction of the spheres (the volume of spheres and the volume of the structure), γ is the surface energy, and D is the sphere diameter. In the systems considered here, the elastic modulus of the particles and their diameters are fixed. Hence

$$\Delta h \propto \frac{\Delta P}{\varphi^4\gamma^{1/3}}, \tag{7}$$

where Δh is the height recovered and ΔP is the pressure removed. As the consolidation load is increased, the packing fraction increases. In Fig. 14, the slope of the response reduces with increasing consolidation, as predicted in Eq. (7). However, the sample elasticity is comparatively weakly dependent on the surface energy. Hence, although the AFM experiments found that the addition of the boundary lubricant resulted in a considerable reduction of the surface energy, it had little influence on the elasticity of the granular material.

V. CONCLUSION

Experiments were conducted to investigate the relationship between particle-particle interaction forces and the shear response of a granular material. A lubricant film of covalently bound organic molecules was used to modify the particle interaction properties. The AFM colloidal probe technique was used to measure the normal and lateral interaction forces of lubricated and unlubricated surfaces at peak contact stresses of up to approximately 120 MPa. The frictional response of the unlubricated surfaces was complicated by the presence of a soft surface gel-like layer. Initially, there was a linear increase of friction with applied load. However, with any subsequent testing over the same wear track, the friction response changed. This behavior is thought to be due to the surface irregularities in the surface gel layer being smeared out, leaving a wear track which allowed a single region of contact between the sphere and flat. It was found that the frictional response could then be modeled reasonably well using the JKR theory of contact mechanics.

The effect of the lubricant film was to significantly reduce the magnitude of the adhesion forces. AFM normal force curves showed almost no attractive force as the surfaces approached, although on retraction, significant interdigitation of the films had to be overcome to separate the surfaces. However, due to the rapid destruction of the lubricant film during friction testing, the lubricating effect of the virgin surfaces proved difficult to quantify. Once destroyed, the frictional response was similar to that of the gel-coated surfaces described above.

The annular shear cell was used to measure the macroscopic effect of the boundary lubricant. Three properties associated with the shear of the sample were studied: the shear strength, the sample contractions on the removal of shear stress, and the sample expansions on the removal of normal stress. The lubricant film had no measurable effect on the sample expansions. However, shear strength and dilation were both reduced. Previous studies have shown that these two properties of granular shear are related. However, this time the two have been linked through variations in the particle tribological properties.

This work highlights the importance (and complexity) of particle contact history in comparisons of local and global granular shear properties. In the AFM experiments, the contact point was controlled and the local contact history known. Hence the effect of surface films and their progressive wear could be mapped. This allowed a number of interesting effects of particle contact mechanics to be studied. However, in bulk measurements of granular shear, the contact interactions are more complex; particle interactions are more random, with ''virgin'' contacts still appearing to dominate the shear properties after 3 mm of travel. The result is that direct, quantitative comparisons between the two sets

of results are very difficult. It will only be through the combination of experimental studies such as this and computer simulations, in which investigators are allowed the freedom to ''look inside'' the granular material, that a complete understanding of local particle tribology in granular shear will be possible.

ACKNOWLEDGMENTS

This research was supported by the Australian Research Council through its individual research grants scheme and in conjunction with the Center for Bulk Solids and Particulate Technologies and the Center for Multiphase Processes.

[1] N. W. Page, M. Yousuff, and C. J. Wauchope, Kona **11**, 147 (1993).
[2] L. C. Y. Chan and N. W. Page, Powder Technol. **90**, 259 (1997).
[3] P. A. Thompson and G. S. Grest, Phys. Rev. Lett. **67**, 1751 (1991).
[4] T. T. Ng and R. Dobry, J. Geotech. Eng. **120**, 388 (1994).
[5] S. M. Wolfrum, J. Mater. Sci. Lett. **7**, 1130 (1988).
[6] S. M. Wolfrum and J. J. Ponjee, J. Mater. Sci. Lett. **8**, 667 (1989).
[7] M. Mullier, U. Tuzun, and O. R. Walton, Powder Technol. **65**, 61 (1991).
[8] G. Binnig, C. F. Quate, and C. Gerber, Phys. Rev. Lett. **56**, 930 (1986).
[9] O. Marti, Phys. Scr. **T49**, 599 (1993).
[10] J. A. Ruan and B. Bhushan, ASME J. Tribol. **116**, 378 (1994).
[11] R. W. Carpick, N. Agrait, D. F. Ogletree, and M. Salmeron, J. Vac. Sci. Technol. B **14**, 1289 (1996).
[12] R. W. Carpick, N. Agrait, D. F. Ogletree, and M. Salmeron, Langmuir **12**, 3334 (1996).
[13] R. W. Carpick and M. Salmeron, Chem. Rev. **97**, 1163 (1997).
[14] J. Colchero, M. Luna, and A. M. Baro, Appl. Phys. Lett. **68**, 2896 (1996).
[15] C. T. Gibson, G. S. Watson, and S. Myhra, Wear **213**, 72 (1997).
[16] W. Ducker, T. Senden, and R. Pashley, Nature (London) **353**, 239 (1991).
[17] W. A. Ducker, T. J. Senden, and R. M. Pashley, Langmuir **8**, 1831 (1992).
[18] Y. I. Rabinovich and R.-H. Yoon, Colloids Surf., A **93**, 263 (1994).
[19] G. Toikka, R. A. Hayes, and J. Ralston, J. Colloid Interface Sci. **180**, 329 (1996).
[20] G. Toikka, R. A. Hayes, and J. Ralston, J. Adhes. Sci. Technol. **11**, 1479 (1997).
[21] S. Biggs and G. Spinks, J. Adhes. Sci. Technol. **12**, 461 (1998).
[22] N. Jaffrezic-Renault and C. Martelet, Sens. Actuators A **32**, 307 (1992).
[23] R. M. Nedderman, *Statics and Kinematics of Granular Materials* (Cambridge University Press, Cambridge, England, 1992).
[24] E. N. Bromhead, Ground Eng. **12**, 40 (1979).
[25] H. Wilms and J. Schwedes, Bulk Solids Handling **5**, 1017 (1985).
[26] R. G. Cain and N. W. Page, in *Proceedings of the 5th International Conference on Bulk Materials Storage, Handling and Transportation, Newcastle, Australia, 1995* (The Institution of Engineers, Australia, 1995), p. 347.
[27] R. G. Cain, N. W. Page, and S. Biggs, J. Colloid Interface Sci. **227**, 55 (2000).
[28] C. M. Mate, M. R. Lorenz, and V. J. Novotny, J. Chem. Phys. **90**, 7550 (1989).
[29] N. Burnham, R. Colton, and H. Pollock, Nanotechnology **4**, 64 (1993).
[30] G. W. McLellan and E. B. Shand, *Glass Engineering Handbook*, 3rd ed. (McGraw-Hill, New York, 1984).
[31] M. J. Adams, in *Fundamentals of Friction: Macroscopic and Microscopic Processes*, edited by I. L. Singer and H. M. Pollock (Kluwer Academic, Dordrecht, 1992), p. 183.
[32] K. Kendall, Nature (London) **319**, 213 (1986).
[33] K. L. Johnson, K. Kendall, and A. D. Roberts, Proc. R. Soc. London, Ser. A **324**, 301 (1971).
[34] F. P. Bowden and D. Tabor, *The Friction and Lubrication of Solids II* (Oxford University Press, Oxford, 1964).
[35] K. L. Johnson, Proc. R. Soc. London, Ser. A **453**, 163 (1997).
[36] M. Enachescu, R. J. A. van den Oetelaar, R. W. Carpick, D. F. Ogletree, C. F. J. Flipse, and M. Salmeron, Tribol. Lett. **7**, 73 (1999).
[37] G. Vigil, Z. Xu, S. Steinberg, and J. Israelachvili, J. Colloid Interface Sci. **165**, 367 (1994).
[38] J. F. Archard, Proc. R. Soc. London, Ser. A **243**, 190 (1957).
[39] J. N. Israelachvili, *Intermolecular and Surface Forces*, 2nd ed. (Academic, London, 1991).
[40] B. J. Briscoe and D. C. B. Evans, Proc. R. Soc. London, Ser. A **380**, 389 (1982).
[41] R. Cain and N. Page, in *ACAM '99: The Second Australasian Congress on Applied Mechanics, Canberra, Australia, 1999* (The Institution of Engineers, Australia, 1999).
[42] R. Cain, N. Page, and S. Biggs (unpublished).
[43] N. W. Page, in *Proceedings of the 5th International Conference on Bulk Materials Storage, Handling and Transportation* [26], p. 409.
[44] S. B. Savage and M. Sayed, J. Fluid Mech. **142**, 391 (1984).
[45] M. A. Koenders and E. Stefanovska, Powder Technol. **77**, 115 (1993).
[46] G. T. Nolan and P. E. Kavanagh, Powder Technol. **76**, 309 (1993).
[47] J. P. Bardet, Mech. Mater. **18**, 159 (1994).
[48] C. Hogue and D. Newland, Powder Technol. **78**, 51 (1994).
[49] K. Kendall, in *Tribology in Particulate Technology*, edited by B. J. Briscoe and M. J. Adams (Hilger, Bristol, 1987), p. 110.